COMPDYN 2015
5th ECCOMAS Thematic Conference on
Computational Methods in Structural Dynamics and Earthquake Engineering
M. Papadrakakis, V. Papadopoulos, V. Plevris (eds.)
Crete Island, Greece, 25–27 May 2015

DEFORMATION CAPACITY OF NON-COMFORMING RC SHEAR WALLS: ANALYTICAL AND NUMERICAL ESTIMATION - TEST VERIFICATION

Christidis K.I.[1], Anagnostopoulou V.V.[1], Trezos K.G. [1], and Zeris C.A.[1]

[1] Laboratory of Reinforced Concrete, School of Civil Engineering
National Technical University of Athens (N.T.U.A.)
5, Iroon Polythechniou, Zografou, 15773, Athens, Greece
e-mail: {christidis, vantua, ctrezos, zeris}@central.ntua.gr

Keywords: RC shear walls, EC8-3, numerical analysis, OpenSees, deformation capacity, experimental verification.

Abstract. *An approach for the analytical prediction of the deformation capacity of reinforced concrete (RC) shear walls in existing buildings, designed with past non conforming seismic regulations is presented. Most modern seismic assessment and redesign provisions include models for the prediction of the capacity of existing RC members. Specifically, Eurocode 8-Part 3 provides semi-empirical and analytical expressions which focus on the estimation of yield and ultimate chord rotation. For this purpose, cross section analyses were carried out using OpenSees platform in order to predict the Moment-Curvature diagram (M-φ) which is thereafter transformed, by analytical expressions, into the final Load-Displacement (P-δ) capacity curve of such members. In addition, numerical simulations were carried out using two alternative element models, available in OpenSees library, in order to directly predict the overall Load-Displacement (P-δ) curve of a shear wall. Both analytical and numerical results were compared with test results from a series of experiments of isolated non conforming RC shear wall elements, which were tested as cantilevers under statically reversed lateral loading in the RC Laboratory of the National Technical University of Athens.*

1 INTRODUCTION

Reinforced concrete (RC) shear walls play an important role in modern seismic design, as they constitute a bracing member capable of contributing to the lateral seismic resistance of the structure. Most modern seismic codes give great attention to the seismic detailing of RC shear walls, trying to secure the flexural behaviour of the member and to reach adequate ductility levels. This is mainly achieved by the configuration of confined boundary elements, which increase the ultimate concrete strain and, therefore, the ductility values, and by a capacity design procedure which leads to high ratios of shear reinforcement, in order to prevent a shear brittle failure.

However, in a lot of countries with high seismic exposure, there is a significant number of existing RC buildings designed according to past seismic regulations, which include shear walls which are non-compliant to modern seismic design and detailing provisions. These non conforming shear walls do not include confined boundary elements and they are characterized by relatively thinner web dimension and low ratios of horizontal or vertical shear reinforcement.

2 LITERATURE REVIEW

An extensive experimental investigation of the behaviour of RC shear walls started taking place in the early 1970s. However, in most cases, the studies were made towards the revision of the applicable regulations at that time, so the conclusions and models arising from this research, which was adopted in the revisions that were effected from these, referred to improved design provisions rather than assessment procedures.

In the next decades, the study of the behavior of RC members began to focus not only on the design but also on the assessment and redesign of existing members. Several models have been developed trying to predict the deformation capacity and the degradation of the shear / flexural strength with inelastic cyclic displacements of existing RC members. Some of these models have been adopted, with some modifications, in modern seismic regulations.

2.1 Analytical assessment models – Plastic hinge analysis

The deformation capacity of reinforced concrete members is commonly defined in currently enforced assessment regulations in terms of the chord rotation (or drift ratio), θ, i.e. the angle between the tangent to the axis at the yielding (assumed fixed) end and the chord connecting that end with the end of the shear span; fixed end effects may also be included in this form of deformation, attributed to effects due to bond deterioration in the region of fixity. Plastic hinge analysis of these rotations relates to the Moment-curvature, M-φ (or Force-deformation, P-δ) envelope of the cyclic response of an RC member.

The ultimate chord rotation at failure, θ_u, can be expressed as the sum of two separated terms: the chord rotation at yielding, θ_y, and the plastic part of the chord rotation, θ_{pl}. Assuming a pure flexural behavior, which means neglecting shear and bond slip effects within the member, the ultimate chord rotation can be expressed as:

$$\theta_u=\theta_y+\theta_{pl}=\varphi_y\frac{L_V}{3}+\left(\varphi_u-\varphi_y\right)L_{pl}\left(1-\frac{L_{pl}}{L_V}\right) \quad (1)$$

where

φ_y is the section curvature at yielding

φ_u is the ultimate curvature at failure

L_V is the length of the shear span ($L_V=M/V$=moment/shear at the end section)

L_{pl} is the plastic hinge length

In the literature, in most cases, the length of the plastic hinge is expressed by empirical or semi-empirical expressions. One of the first is the one of Paulay and Priestley [1]:

$$L_{pl}=0.08L_V+0.022d_bf_y \tag{2}$$

where the second term is the contribution of slippage of the longitudinal rebars expressed by the product of the diameter d_b and the yield stress, f_y, of the longitudinal tension reinforcement.

Along the same premise Panagiotakos and Fardis [2] proposed a modified expression for plastic hinge length, L_{pl}, (Eq.(3)), trying to fit Eq.(1) to the results from a large experimental database. Panagiotakos and Fardis [2] distinguished the cases of monotonic and cycling loading, noting that the shear, bond slip and tension stiffening effects should be taken into account via the plastic hinge length expressions:

For monotonic loading

$$L_{pl}=0.18L_V+0.021a_{sl}d_bf_y \tag{3a}$$

For cyclic loading

$$L_{pl}=0.12L_V+0.014a_{sl}d_bf_y \tag{3b}$$

where a_{sl} equals 1 or 0 depending on whether slippage of the longitudinal steel is possible or not.

Based on an extended experimental database, Biskinis [3], proposed a new parametric expression for calculating the plastic hinge length, L_{pl}, as a function of geometrical characteristics only, taking into account shear and bond slip effects within the expression of ultimate chord rotation. This empirical model gradually evolved to its final form in Biskinis and Fardis [4]-[5], Grammatikou [6] and Grammatikou et al. [7] as:

$$\theta_u=\theta_y+a_{sl}\Delta\theta_{u,slip}+\left(\varphi_u-\varphi_y\right)L_{pl}\left(1-\frac{0.5L_{pl}}{L_V}\right) \tag{4}$$

In Eq.(4) θ_y is the chord rotation at yielding and $\Delta\theta_{u,slip}$ is the rotation due to slippage from yielding until failure, calculated from Eq.(5) and Eq.(6a, 6b), respectively:

$$\theta_y=\varphi_y\frac{L_V+\alpha_V z}{3}+0.0006\left(1+\frac{7}{6}\frac{h}{L_V}\right)+a_{sl}\varphi_y\frac{d_bf_y}{8\sqrt{f_c}} \tag{5}$$

where

$\alpha_V z$ is the tension shift of the bending moment diagram due to shear

z is the length of the internal flexural lever arm, taken equal to $0.8h$ in walls with rectangular section (h is the cross-section depth),

α_V=1 if shear cracking is expected to precede flexural yielding at the end section (i.e. if $M_y>L_VV_{R,c}$); otherwise α_V=0, where $V_{R,c}$ is the shear resistance of the member considered without shear reinforcement according to Eurocode 2 - Part 1-1 [8]

f_c is the concrete compressive strength

According to the model, $\Delta\theta_{u,slip}$ can be calculated as:

For monotonic loading

$$\Delta\theta_{u,slip}=9.5d_b\varphi_u \tag{6a}$$

For cyclic loading

$$\Delta\theta_{u,slip}=5.5d_b\varphi_u \tag{6b}$$

and L_{pl} can be calculated as:

For monotonic loading with or without conforming seismic detailing

$$L_{pl}=h\left[1.1+0.04min(9;\frac{L_V}{h})\right] \tag{7a}$$

For cyclic loading with conforming seismic detailing

$$L_{pl}=0.3h\left[1.0+\frac{1}{6}min(9;\frac{L_V}{h})\right] \tag{7b}$$

Note that there is a direct interaction between L_{pl} and φ_u. Thus, each expression for calculating L_{pl} matches to a specific model for calculating the concrete compressive strength and the corresponding ultimate concrete strain. The model of Eq.(4) to Eq. (7) is based on the Newman and Newman [9] model for the confined concrete, according to which the compressive strength of the confined concrete, f_{cc}, is calculated as:

$$f_{cc}=f_c\left[1+3.7\left(\frac{a\rho_{sx}f_{yw}}{f_c}\right)^{0.86}\right] \tag{8}$$

where

$\rho_{sx}=A_{sx}/bs_h$ is the ratio of transverse steel parallel to the direction x of loading (A_{sx} is the stirrup reinforcement area and s_h is the stirrup spacing),

f_{yw} is the stirrup yield strength (MPa) and

α is the confinement effectiveness factor.

The strain at maximum strength, e_{cc0}, can be calculated as (Fardis [10]):

$$\varepsilon_{cc0}=\varepsilon_{c0}\left[1+5\left(\frac{f_{cc}}{f_c}-1\right)\right] \tag{9}$$

The ultimate concrete strain, ε_{ccu}, is taken as (Biskinis and Fardis [5]):

For monotonic loading

$$\varepsilon_{ccu}=0.0035+\left(\frac{10}{h_0}\right)^2+0.57\frac{a\rho_s f_{yw}}{f_{cc}} \tag{10a}$$

For cyclic loading

$$\varepsilon_{ccu}=0.0035+\left(\frac{10}{h_0}\right)^2+0.40\frac{a\rho_s f_{yw}}{f_{cc}} \tag{10b}$$

where

h_o is the confined core height (in mm): In case the element does not include a confining detailing configuration, the value h_o is replaced by the cross-section height, h, and the third term of Eq.(10) is set equal to zero.

2.2 Eurocode 8 - Part 3 provisions

Eurocode 8 - Part 3 (EC8-3) [11], [12] in Annex A proposes models for the performance assessment of reinforced concrete members that refer to their deformation capacity, in chord rotation terms, and their shear strength. EC8-3 defines three different limit states, indicating the state of damage of the concrete member – Damage Limitation (DL), Significant Damage (SD) and Near Collapse (NC).

The value of the chord rotation, θ_y, in the DL limit state for rectangular walls is given in Eq.(11) and it corresponds to the yielding moment capacity, M_y.

$$\theta_y=\varphi_y\frac{L_V+\alpha_V z}{3}+0.0013+\varphi_y\frac{d_b f_y}{8\sqrt{f_c}} \tag{11}$$

The value of the ultimate (total) chord rotation, θ_u, in the NC limit state is given in Eq.(12) and it corresponds to the ultimate moment capacity, M_u.

$$\theta_u=\frac{1}{\gamma_{el}}0.016(0.3^{\nu})\left[\frac{max(0.01;\omega')}{max(0.01;\omega)}f_c\right]^{0.225}\left(min\left(9;\frac{L_V}{h}\right)\right)^{0.35}25^{\left(\alpha\rho_{sx}\frac{f_{yw}}{f_c}\right)}(1.25^{100\rho_d}) \tag{12}$$

where:
γ_{el} is equal to 1.50 for primary seismic elements and to 1.00 for secondary seismic elements,
$\nu=N/bhf_c$ (b is the width of compression zone, N is the axial force positive for compression),
ω, ω' are the mechanical reinforcement ratios of the tension (including the web reinforcement) and compression, respectively, longitudinal reinforcement,
ρ_d is the steel ratio of diagonal reinforcement (if any), in each diagonal direction.

Note that for shear walls the above value must be multiplied by 0.58, while, specifically for members without seismic detailing, it must be also divided by 1.2. The intermediate value of the chord rotation, θ_{SD}, in the SD limit state may be taken as the $0.75\theta_u$.

Alternatively, EC8-3 proposes an analytical expression for calculating the ultimate chord rotation (Eq.(13)). Note that the specific expression is applicable only for the assessment of existing members with seismic detailing; no proposal for members with poor seismic detailing is made.

$$\theta_u=\theta_y+\left(\varphi_u-\varphi_y\right)L_{pl}\left(1-\frac{0.5L_{pl}}{L_V}\right) \tag{13}$$

where the plastic hinge length, L_{pl}, depends on the constitutive model for confined concrete:
For the confinement model included in Eurocode 2 - Part 1-1 [8]

$$L_{pl}=0.1L_V+0.17h+0.24\frac{d_b f_y}{\sqrt{f_c}} \tag{14a}$$

For a confinement model proposed in EC8-3 (based on Newman and Newman model [9])

$$L_{pl}=\frac{L_V}{30}+0.20h+0.11\frac{d_b f_y}{\sqrt{f_c}} \tag{14b}$$

The above confinement model of EC8-3 adopts Eq.(8) and (9) for f_{cc} and ε_{cc0}, respectively, and proposes that the ultimate concrete strain ε_{ccu} can be calculated as:

$$\varepsilon_{ccu}=0.004+0.5\frac{a\rho_s f_{yw}}{f_{cc}} \tag{15}$$

From the literature review, a main conclusion could be derived: Each empirical expression for predicting the plastic hinge length can be applied only in accordance with a certain model for calculating the ultimate curvature. The fact that the database, on which the above models were calibrated, comprises primarily members with seismic detailing, leads to the result that these expressions have application mainly (or only) to members with seismic detailing (e.g. EC8-3).

2.3 Numerical methods

Apart from the analytical models previously described, efforts have been made towards the development of reliable numerical methods for simulating the monotonic and cyclic behavior of RC members. In most cases these methods are based on Finite Element Methods (FEM).

An alternative numerical model which specially focuses on the simulation of RC shear walls is the one proposed in Massone et al. [13]. The base of the above model is a macroscopic fiber-based model, referred as Multiple-Vertical-Line-Element-Model (MVLEM), proposed by Vulcano et al. [14]. According to this approach an RC shear wall is modeled as a stack of Multiple-Vertical-Line-Elements (MVLEs), placed one upon the other. Each MVLE is simulated by a series of uniaxial elements connected to rigid beams, in order to capture the flexural component, and by a horizontal spring in order to capture the shear behavior. However, this simulation does not take into account the shear-flexure interaction.

In view of this limitation, Massone et al. [13] and Orakcal et al. [15] suggested an improved model, by assigning a shear spring for each uniaxial element, achieving a RC membrane behavior for each element.

3 EXPERIMENTAL PROCEDURE

In order to evaluate both analytical and numerical models presented within this paper, as well as the aforementioned code provisions, a comparison of analytical predictions with experimental results was carried out. The experimental process included the testing of a series of four RC shear walls. This testing forms part of a general experimental program, which is taking place in the RC Laboratory of the National Technical University of Athens (NTUA), whose scope is the assessment and strengthening of existing non-conforming RC shear walls. Two of the specimens (W_9 and W_{11}) were previously presented in Christidis et al. [16], while the other two (W_7 and W_{13}) are described herein.

3.1 Specimens characteristics

Walls W_7 and W_{13} represent a typical modern RC shear wall designed according to Eurocode provisions and a typical existing non-conforming RC shear wall, respectively. Specimens W_9 and W_{11} also represent non-conforming walls but, in addition, a configuration of open stirrups was added in order to prevent the buckling of compressive reinforcement, found often to reduce the bearing capacity of the wall prematurely; in this way the influence of shear reinforcement can be evaluated directly. The dimensions and the reinforcement configuration of all specimens are shown in Fig.1 and they are summarized in Table 1.

	Concrete compression strength f_c (MPa)	Reinforcement yield/failure f_y/f_u (MPa)		Longitudinal reinforcement ratio ρ_{tot} (‰)	Transverse (shear) reinforcement ratio ρ_w (‰)
		Longitudinal Reinforcement	Stirrups		
Wall W_7	32.12	D10:604/705 –D8:588/681	588/681	14.33	6.69
Wall W_9	31.12	580/670	588/681	12.06	2.01
Wall W_{11}	31.12	580/670	568/654	12.06	1.13
Wall W_{13}	25.37	580/670	568/654	12.06	1.13

ρ_{tot}=Area sum of longitudinal reinforcement/cross section area=$\Sigma A_{s,L}/(b_w*h)$
ρ_w=Area sum of stirrup/(wall width*stirrups distance)=$\Sigma A_{s,w}/(b_w*s)$

Table 1: Reinforcement ratios and material properties of the specimens considered.

It should be noted at this point that the flexural inelastic deformations, presented in detail in Section 2 (especially the ultimate values) can be attained provided that the structural

member has not previously reached its shear strength capacity, whose value can be calculated according to EC8-3 provisions. Walls W_{11} and W_{13} include such a shear reinforcement ratio that intentionally leads to a reduced value of shear capacity, typical of existing wall elements, so that the flexural behavior of the wall cannot be attained (see also Christidis et al. [16]). However, the expected brittle-shear behavior of the specimens was not verified by the test results (as also explained later), since all the specimens exhibited their flexural capacity and significant higher values of corresponding lateral displacement, not affected by the different reinforcement ratios. Thus, the evaluation of displacement capacity of Walls W_{11} and W_{13} was conducted in flexural terms: the investigation of the reliability of proposed models for calculating the shear strength capacity is beyond the scope of this paper.

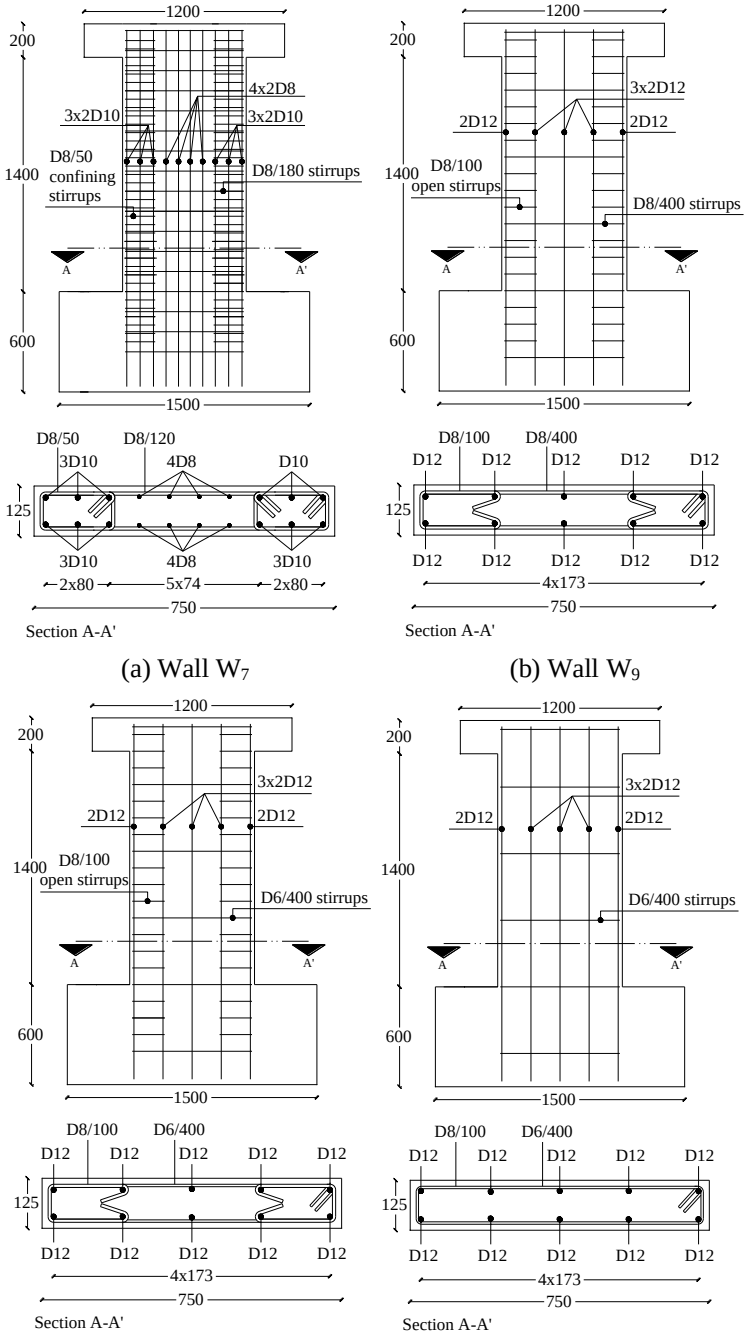

(a) Wall W_7 (b) Wall W_9

(c) Wall W_{11} (d) Wall W_{13}

Figure 1: Reinforcement configuration of specimens (in mm).

3.2 Experimental procedure

The specimens were tested as cantilevers under static cyclic loading. During the testing procedure, a displacement control method was adopted, including an initial displacement of ±10 mm with steps of 10 mm until failure. Three cycles of each displacement group were applied: the time history of the loading is shown in Fig.2.

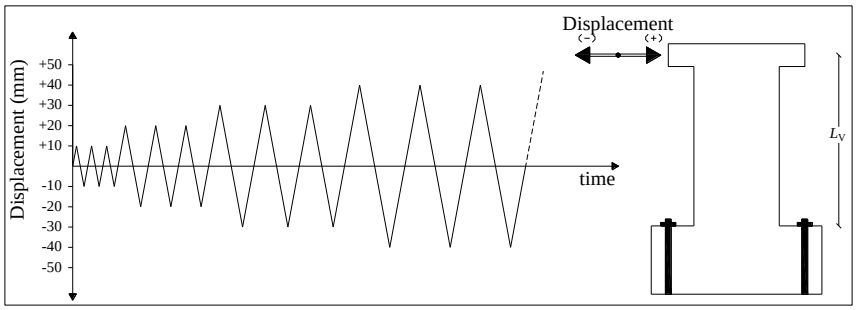

Figure 2: Time history of loading of specimens.

3.3 Experimental results – failure modes

The experimental results are presented in Fig.12 (together with analytical and numerical predictions) in the form of the Load-displacement diagram, *P-δ*, where *δ* refers to the displacement at the top of each specimen. In Fig.3, the cracking pattern is shown at the end of the experimental procedure.

(a) Wall W_7

(b) Wall W_9

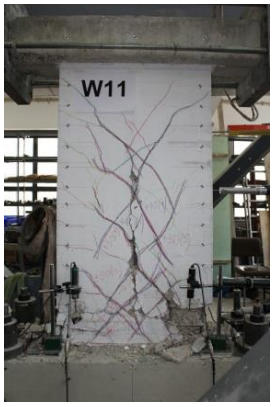

(c) Wall W_{11}

(d) Wall W_{13}

Figure 3: Cracks at the end of the experiment (at displacement 0.00mm).

As concluded from the experimental results, low ratios of shear reinforcement seem to affect neither the bearing capacity nor the top displacement capacity of walls. All four specimens reached approximately their flexural bearing capacity, while in most cases they exhibited a flexural post-yield behavior followed by significant values of ductility, except of Wall W_{13} which exhibited a descending post-yield branch, which, however, is attributed to the premature buckling of the compressive longitudinal reinforcement. Contrariwise, low ratios of shear reinforcement seem to determine the crack mode of walls, as in cases of walls W_{11} and W_{13} with low ratios of shear reinforcement the formation of significant inclined X cracks was observed.

4 ANALYTICAL AND NUMERICAL ESTIMATION

EC8-3 provisions (both empirical and analytical) and Eq.(4) to Eq.(10) model (for cyclic loading) were applied for all the four specimens and compared with the experimental results. In order to apply the analytical or empirical models cross-section analyses (CS) were preceded in OpenSees platform [17]. In addition to the analytical predictions of section response, numerical simulations were also carried out at the element level, again using the OpenSees platform [17], which were also compared with experimental results.

4.1 Materials

As previously described, each one of the analytical models can be applied only in accordance with a specific concrete constitutive law. Thus, Eq.(8), (9) and (15) were applied to describe the confined concrete, in order to evaluate the EC8-3 ([11], [12]) provisions while Eq.(8), (9) and (10) were applied in order to evaluate the model of Eq.(4) to Eq.(10). For the numerical analysis at the element level the EC8-3 confined concrete model was applied. Especially in Wall W_{13}, where only unconfined concrete was used across the cross-section, the two previous models were used with a=0 for the unconfined core concrete. Note that in both models the value of strain at failure ε_{ccu} (or e_{cu}) corresponds to a concrete strength equal to $0.85f_{cc}$ (or $0.85f_c$). Finally, the Kent and Park model [18] was used to describe the unconfined cover concrete constitutive law in all cases (Fig.4).

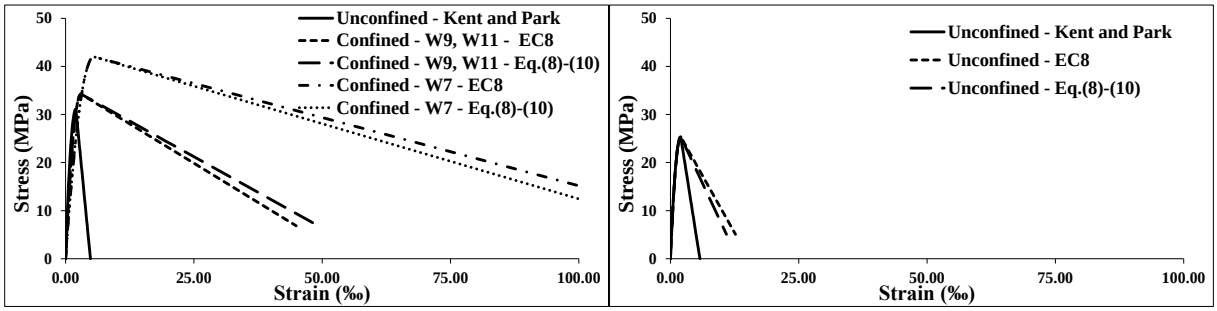

(a) Concrete f_c=31.12MPa (Walls W_7, W_9, W_{11}) (b) Concrete f_c=25.37MPa (Wall W_{13})

Figure 4: Concrete stress-strain (σ-ε) curves in compression.

In all cases (cross-section and element level) the analyses were carried out ignoring the tension strength of concrete, so a *Concrete_01-Zero Tensile Strength* material was used in OpenSees for the concrete. Chang and Mander [19] model was used to describe the reinforcing steel constitutive law including the buckling of compressive bars according to Dhakal and Maekawa [20] model (OpenSees: *Reinforcing Steel Material*) (Fig.5). The buckling of compressive steel depends mainly on the ratio *L/D*, where *L* is the unsupported bar length and *D* is the diameter of the reinforcing bar. The influence of buckling to the

Moment - Curvature diagram is shown indicatively in Fig.6a, where the Moment-Curvature diagram of wall W_{13} is derived from a cross-section analysis for three different cases, namely without buckling and with buckling, for L/D = 8.33 and L/D = 33.33.

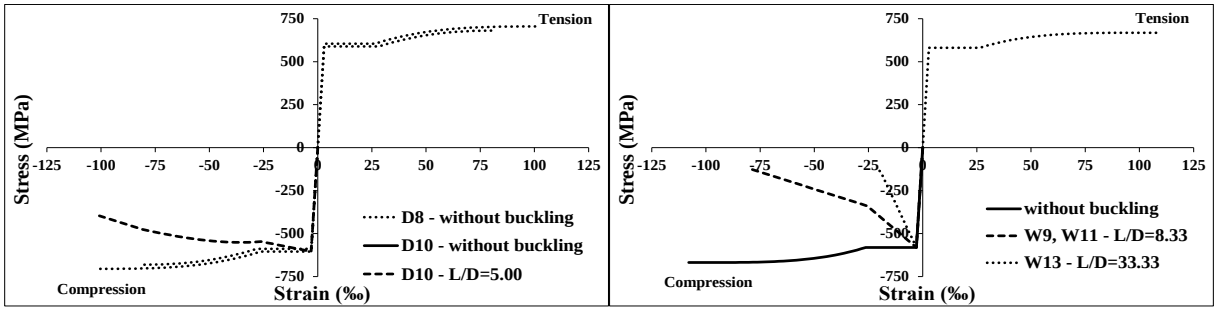

(a) Reinforcing bars D10 and D8 in Wall W_7 (b) Reinforcing bar D12 in Walls W_9, W_{11} and W_{13}

Figure 5: Reinforcing bars stress-strain (σ-ε) curves.

Another parameter which influences the reduction of steel stress due to buckling is the parameter *a* (Dhakal and Maekawa [20]). As Dhakal and Maekawa [20] state, the value of *a* is found to be 0.75 for elastic–perfectly plastic bars and 1.0 for bars with continuous linear hardening. Thus, for bars with a limited hardening range, *a* should be chosen between 0.75 and 1. Dhakal and Maekawa [21] recommend a system of equations for calculating the parameter *a*. In the case of reinforcing bars *D*10 and *D*12 of the wall models herein, the above equations lead to values 0.777 and 0.767, respectively, so the lower bound of 0.75 was adopted. Besides, the value of parameter *a* does not seem to have a significant influence on the overall Moment-Curvature of the cross-section, as also shown in Fig.6b.

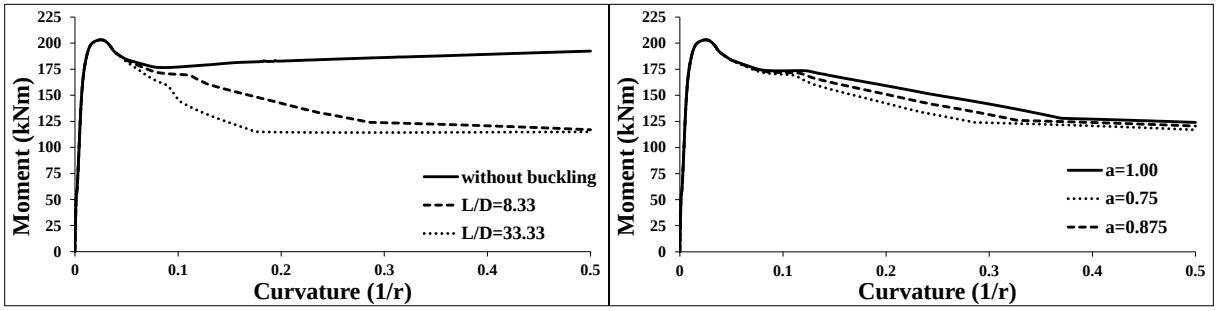

(a) Influence of L/D for constant a=0.75 (b) Influence of a for constant L/D=8.33

Figure 6: Influence of buckling parameters L/D and a to the Moment Curvature diagrams of Wall W_{13}.

4.2 Analytical estimation

In order to apply the analytical equations a conventional yielding point was used, obtained from the bilinearization of the Moment-Curvature diagram, M-φ, using an equivalent bilinear curve (elastic-perfectly plastic), where the initial elastic stiffness is defined from the first yield point (M_{y1}, φ_{y1}). The conventional yield point (M_y, φ_y) was derived by equating the area (energy) of the two curves. Note that the ultimate curvature, φ_u, is taken as the one corresponding to a percentage 20% loss of the bearing capacity. The Moment-curvature diagrams derived from the cross-section analysis in OpenSees and their equivalent bilinear counterparts are summarized in Fig.7; the Load-displacement (P-δ) curves derived from the application of the analytical expressions above, using the M-φ curves are discussed later on, in comparison with numerical and experimental results (see also Fig.12).

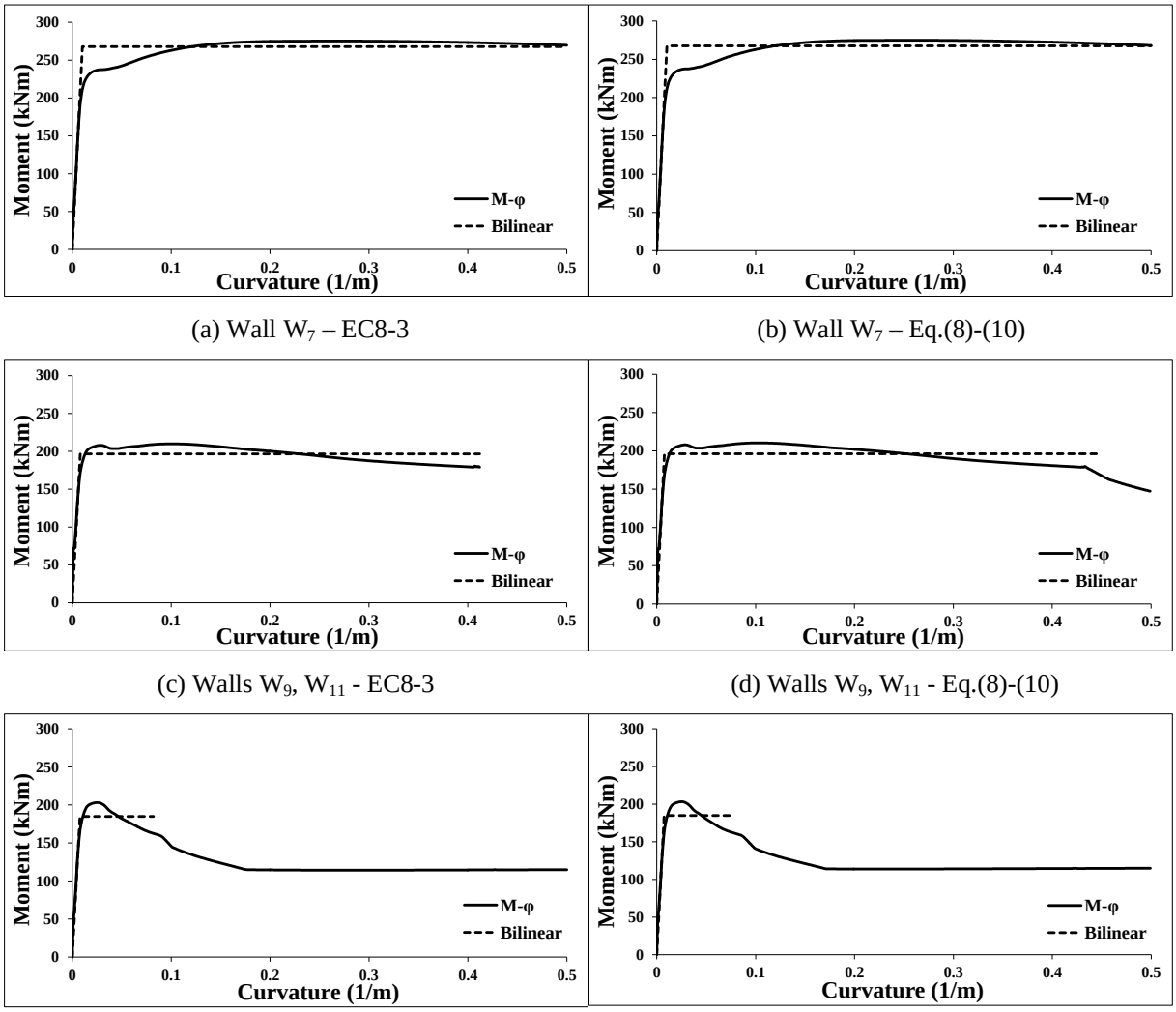

(a) Wall W_7 – EC8-3

(b) Wall W_7 – Eq.(8)-(10)

(c) Walls W_9, W_{11} - EC8-3

(d) Walls W_9, W_{11} - Eq.(8)-(10)

(e) Wall W_{13} – EC8-3

(f) Wall W_{13} – Eq.(8)-(10)

Figure 7: Moment curvature diagrams (M-φ).

4.3 Numerical analysis

In addition to the previous analytical approach, numerical simulations were carried out using OpenSees platform to predict the experimental response. The simulation of the RC shear wall was held in two alternative ways. The first one was by using the Displacement-Based Beam-Column Element, which considers the spread of plasticity along the element height. This element is a flexural element model based on internal interpolation of deformations, while relying only on the flexural characteristics of the cross-section (i.e. geometry, longitudinal reinforcement, material laws) for the response evaluation; therefore, it does not take into account the shear component neither in the evaluation of the total strength nor the total displacement (also, fixed end effects were not included at the base end). Thus, via this model, it is possible to evaluate the differences in the total P-δ behavior of the wall only due to flexural changes in the cross section, i.e. the influence of the confinement and the influence of the buckling of the compressive longitudinal bars, but not the influence that different shear reinforcement ratios have.

On the other hand, the influence of the shear reinforcement can be simulated by using the Flexure-Shear Interaction Displacement-Based Beam-Column Element available in OpenSees that takes into account the interaction between flexure and shear components, based on

Massone et al. [13] work. The specific model is sensitive to three modelling factors: the discretization of the cross-section in *n* strips, the number of subelements, *m*, along the wall height and the value of the parameter *c*, which is the center of rotation (or the center of gravity of the curvature distribution) in each subelement.

The discretization of the cross section in *n* strips for each element was performed in order to achieve the best simulation of the actual test cross-section configuration, i.e. the exact place of the rebars and the transitions between confined and unconfined concrete (Fig.8a,b).

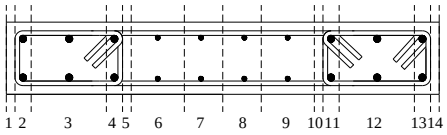

(a) Discretization in *n* strips - Wall W_7

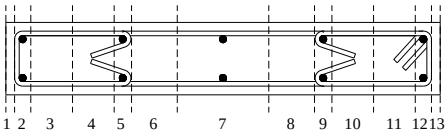

(b) Discretization in *n* strips - Walls W_9, W_{11}, W_{13}

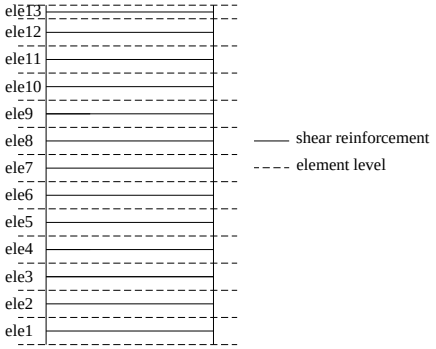

(c) Discretization in *m* subelements - Wall W_7

Figure 8: Modelling of walls in OpenSees.

As far as the number of subelements, *m*, along the wall height (see indicatively Fig.8c), it was decided to divide the total height according to the distance of the horizontal shear reinforcement. Thus, Wall W_7 was divided in m=13 element (at 0.12m) while Walls W_9, W_{11} and W_{13} were divided in m=4 elements (at 0.40m). Each of these elements contains a constant area of shear reinforcement which, divided by the height of each m_i element and the wall width, *b*, gives the actual shear reinforcement ratio, ρ_w, of each shear wall (see also Table 1). As Orakcal et al. [15] state, "*increasing the number of uniaxial elements or the number of MVLEs along wall height does not change significantly the prediction of the global P-δ response*". On the other hand, "*use of more MVLEs along wall height is valuable in terms of obtaining more detailed information on responses at a given location*". So from this point of view, using only m=4 elements for walls W_9, W_{11} and W_{13} was considered as inadequate. However, it was observed that, increasing the number of MVLEs while trying to keep the shear reinforcement ratio constant and equal to the actual so as not to deviate from the actual wall model, led to the use of subelements with less or even no shear reinforcement. In both cases the *P-δ* analysis results were poor, as shown in Fig.9a, without significantly influencing the local behavior *(*flexural *M-φ* or shear *V-γ)*, so the number m=4 elements was adopted herein.

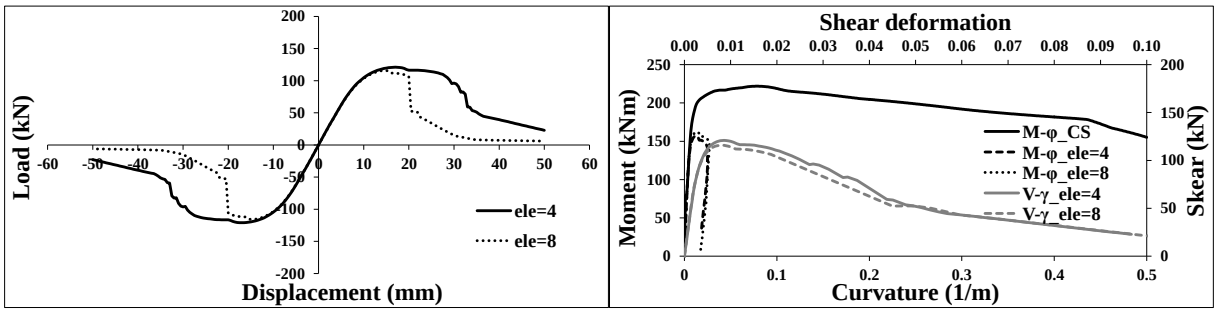

(a) *P-δ* curves

(b) *M-φ* and *V-γ* curves

Figure 9: Comparison of different element number for Wall W_{11}.

Finally, regarding the location of the center of rotation, a value c=0.4 was recommended by Vulcano et al. [14], however, using a large number of MVLEs along wall height, diminishes the influence of this parameter on the predicted response (Orakcal et al. [15]). However, applying the value c=0.4 in wall W_7, although it did not affect significantly the overall P-δ response (Fig.10a), led to an overestimated M-φ diagram compared to the one obtained from a cross section analysis (Fig.10b). Thus, a value of c=0.5 was adopted in this study, which led to a M-φ curve closer to the one of the cross-section analysis.

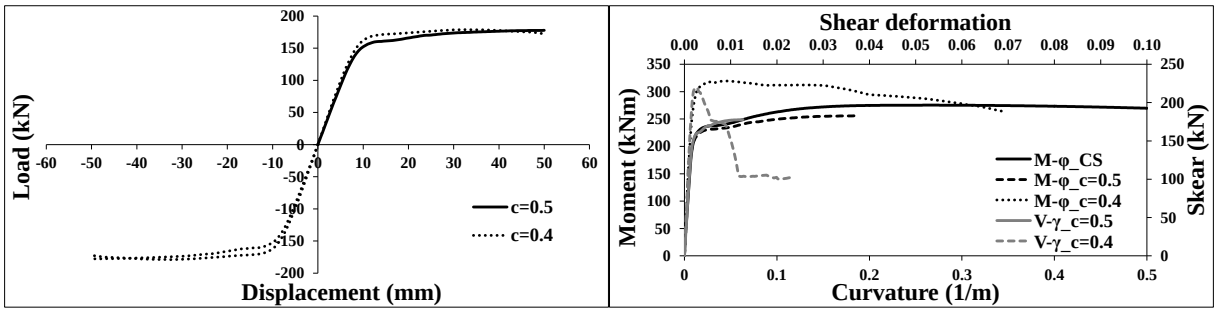

(a) P-δ curves (b) M-φ and V-γ curves at the bottom element

Figure 10: Comparison of c=0.4 and c=0.5 for Wall W_7.

All the flexural (curvature φ) and shear (γ) deformations are summarized in Fig.11.

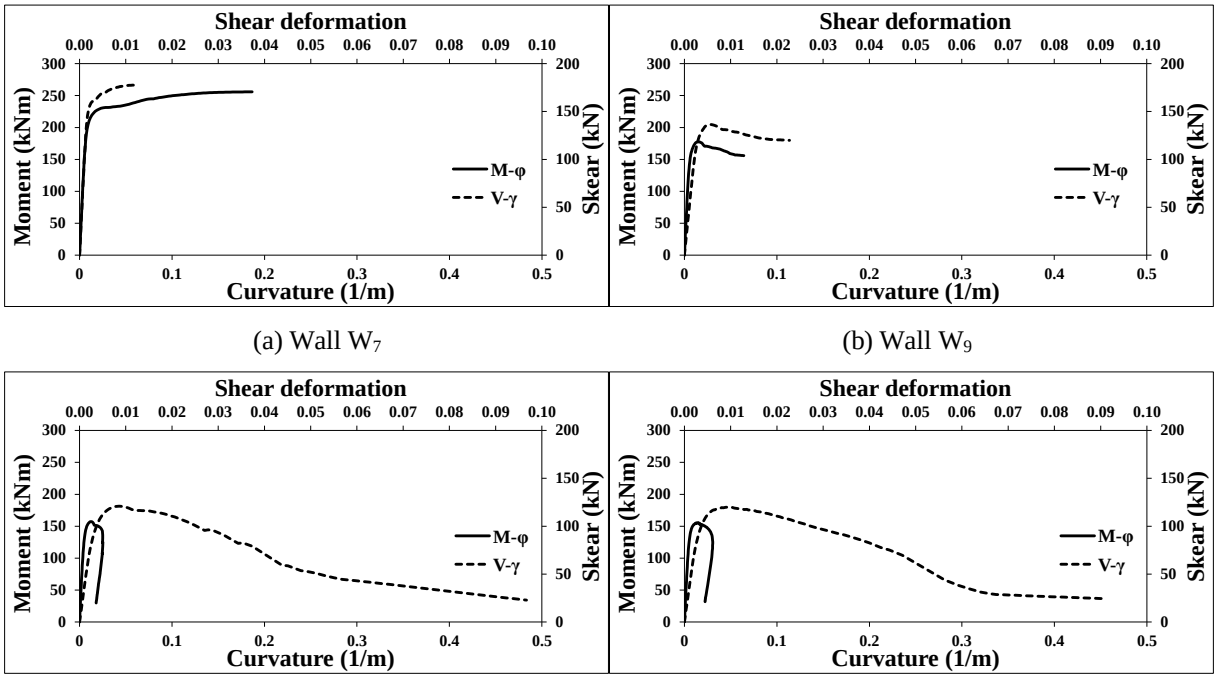

(a) Wall W_7 (b) Wall W_9

(c) Wall W_{11} (d) Wall W_{13}

Figure 11: Flexural (M-φ) and shear (V-γ) deformations for Flexural-shear analysis (c=0.5) at the bottom element.

As shown in Fig.11 the total deformation, δ, is attributed to the interaction between flexural and shear deformations. As a result shear deformation determines the overall displacement capacity of the walls (W_{11} and W_{13}) with low shear reinforcement ratio.

5 EXPERIMENTAL VERIFICATION

The analytical and numerical models presented within this paper are compared with the experimental results, in the form of comparisons of the corresponding *P-δ* diagrams (Fig.12), where *δ* refers to the lateral displacement of the top (at 1.5m) of the wall.

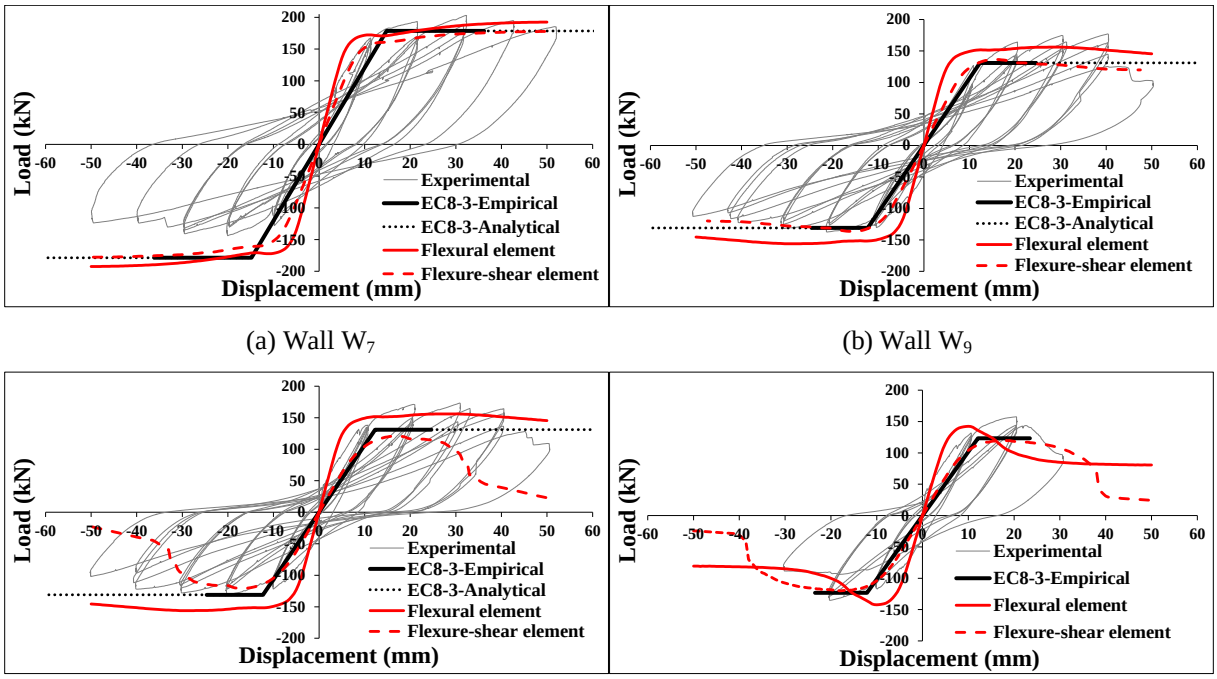

(a) Wall W_7 (b) Wall W_9

(c) Wall W_{11} (d) Wall W_{13}

Figure 12: Load-displacement, *P-δ*, curves of specimens (analytical, numerical and experimental results).

All methods (analytical and empirical) were considered in wall W_7 which represents a conforming shear wall designed according to modern seismic provisions. On the contrary, in Wall W_{13} only the empirical EC8-3 method was considered, as the specific specimen represents a typical non conforming wall without seismic detailing, where analytical models have no application. As far as specimens W_9 and W_{11} are concerned, which constitute an intermediate case, analytical methods were considered for both walls, but the factor 1.2 for non conforming shear walls was conservatively used within the calculations using the empirical methods. Note that in Fig.12 above, the Eq.(4) to Eq.(10) analytical model is not superimposed, since it yields results very similar to the one of EC8-3(analytical). Both analytical methods seem to estimate with high accuracy the deformation capacity of the test shear walls, as they lead to high ductility levels. On the contrary, the empirical method of EC8-3 seems to underestimate the deformation capacity in most test cases.

As shown in Fig.12, the Flexural element seems to estimate with quite good accuracy the overall *P-δ* response of the walls. As mentioned before, the specific model cannot take into account the shear component, consequently, it is not affected by the negative influence of inadequate shear reinforcement in cases of Walls W_{11} and W_{13}; theoretically, for these walls a premature shear failure is expected. However, such a shear failure is not verified by the experimental results, something which is consistent with the results of the displacement based flexural model prediction.

On the other hand, the theoretically more accurate Flexure-shear interaction element seems to underestimate the behavior of the lightly reinforced (in shear) walls W_{11} and W_{13}, as the numerical analysis leads to significantly lower values, both in load and top displacement

terms. However, it is noted that the Flexure-shear interaction element analysis led to stiffness values, until approximately the yielding point, closer to the experimental ones, something which was expected, as the shear component is added to the total displacement value.

6 CONCLUSIONS

Four reinforced concrete shear walls were tested under static cyclic loading. As concluded from the experimental results, low ratios of shear reinforcement seem to affect neither the bearing capacity nor the deformation capacity of these walls. All the specimens reached a maximum load close to their flexural capacity, while in most cases they exhibited a flexural post yield behavior, followed by significant values of ductility. The low ratios of shear reinforcement seem to influence the cracking pattern of the walls, which was characterized by the formation of significant inclined cracks, which, however did not lead to a loss of bearing capacity. The effect of buckling of the compressive longitudinal reinforcement appears intensely in Wall W_{13} which exhibited a descending post-ultimate branch.

The experimental results were compared with the provisions provided in EC8-3, and with the Eq.(4) to Eq.(10) model proposed in the literature. Both analytical models seem to estimate with accuracy the behavior of RC shear walls, while the empirical method of EC8-3 underestimates the ultimate deformation capacity and leads to lower displacement values than the experimental ones, being however on the safe side. Note that within this paper the equations for estimating the shear strength, which often indicate prior brittle failure and, therefore, poor deformation capacity, were not evaluated. As the experimental behavior seems not to be significantly affected by the presence of low shear reinforcement, the comparisons was conducted in flexural terms.

Finally, the experimental results were compared with numerical analyses conducted with two alternative methods – by using a flexural displacement element type and by using a flexural-shear interaction displacement element type. Between the two types of elements the flexural one seems to estimate more accurately the overall P-δ behavior of the walls, while the flexural-shear interaction element estimates better the initial stiffness until yielding. However, the latter element predicts a prior brittle shear failure in the case of the two lightly reinforced walls W_{11} and W_{13}, something which was not confirmed by the experimental results.

REFERENCES

[1] T. Paulay, M.J.N. Priestley, *Seismic design of reinforced concrete and masonry buildings*. John Wiley & Sons, Inc. 1992.

[2] T.B. Panagiotakos, M.N. Fardis, Deformations of reinforced concrete members at yielding and ultimate. *ACI Structural Journal*, **98**, 135–148, 2001.

[3] D. Biskinis, *Strength and deformation capacity of reinforced concrete members with or without strengthening.* PhD Dissertation, University of Patras, 2007 (in Greek).

[4] D. Biskinis, M.N. Fardis, Deformations at flexural yielding of members with continuous or lap-spliced bars. *Structural Concrete*, **11**,127-138, 2010.

[5] D. Biskinis and M.N. Fardis, Flexure-controlled ultimate deformations of members with continuous or lap-spliced bars. *Structural Concrete*, **11**,93-108, 2010.

[6] S. Grammatikou, *Strength, deformation capacity and failure modes of reinforced concrete shear walls under seismic loading.* MSc Dissertation, University of Patras, 2013 (in Greek).

[7] S. Grammatikou, D. Biskinis, M.N. Fardis, Strength, deformation capacity and failure mode of RC walls in cyclic loading. *4th International fib Congress and Exhibition*, Mumbai, India, February 10-13, 2014.

[8] CEN Eurocode 2: *Design of concrete structures - Part 1-1: General rules and rules for buildings (EN 1992-1-1)*. European Committee for Standardization, Brussels, Belgium, 2004.

[9] K. Newman, J. B. Newman, Failure Theories and Design Criteria for Plain Concrete. *Proc., Int. Civil Engrg. Mat. Conference on Structure, Solid Mech. and Engrg. Des. Wiley Interscience*, New York, NY, pp. 936-995, 1971.

[10] M.N. Fardis, *Seismic Design, Assessment and Retrofitting of Concrete Buildings Based on EN-Eurocode8*. Springer Dordrecht Heidelberg, 2009.

[11] CEN Eurocode 8: *Design of Structures for Earthquake Resistance - Part 3: Assessment and Retrofitting of Buildings (EN 1998-3)*. European Committee for Standardization, Brussels, Belgium, 2005.

[12] CEN Eurocode 8: *Design of Structures for Earthquake Resistance - Part 3: Assessment and Retrofitting of Buildings (EN 1998-3:2005/AC).* European Committee for Standardization, Brussels, Belgium, 2010.

[13] L.M. Massone, K. Orakcal, J.W. Wallace, Shear-Flexure Interaction for Structural Walls, *ACI Special Publication*, ***236***, 127- 150, 2006.

[14] A. Vulcano, V.V Bertero, V. Colotti, Analytical Modelling of R/C Structural Walls. *9th World Conference on Earthquake Engineering*, Kyoto – Tokyo, Japan, August 2-9, 1988.

[15] K. Orakcal, L.M. Massone, J.W. Wallace, *Analytical Modeling of Reinforced Concrete Walls for Predicting Flexural and Coupled– Shear-Flexural Responses*. PEER Report 2006/2007, Pacific Earthquake Engineering Research Center, College of Engineering, University of California, Berkeley, 2006.

[16] K. Christidis, E. Vougioukas, K.G. Trezos, Deformation capacity of older RC shear walls: Experimental assessment and comparison with Eurocode 8 – Part 3 Provisions, M.A. Ansal and M. Nurlu eds. *2nd European Conference on Earthquake Engineering and Seismology*, Istanbul, Turkey, August 25-29, 2014.

[17] F. McKenna, G.L. Fenves, B. Jeremic, M.H. Scott, *OpenSees Command Language Manual*, 2007. http://opensees.berkeley.edu.

[18] D.C. Kent, R. Park, Flexural members with confined concrete. *Journal of the Structural Division, Proc. of the American Society of Civil Engineers,* **97(ST7),** 1971.

[19] G.A. Chang, J.B. Mander, *Seismic Energy Basic Fatigue Damage Analysis of Bridge Columns: Part I – Evaluation of Seismic Capacity*. Technical Report NCEER-94-0006, State University of New York at Buffalo, 1994.

[20] R.P. Dhakal, K. Maekawa, Modeling for Post-yield Buckling of reinforcement. *ASCE Journal of Structural Engineering,* **128**, 1139-1147, 2002.

[21] R. Dhakal, K. Maekawa, Path-dependent cyclic stress–strain relationship of reinforcing bar including buckling. *Engineering Structures* **24,** 1383–1396, 2002.